Available online at www.sciencedirect.com
ScienceDirect
Journal of Power Sources 177 (2008) 404–411
JOURNAL OF POWER SOURCES
www.elsevier.com/locate/jpowsour

Transient behavior of water generation in a proton exchange membrane fuel cell

Lixing Hao [a,b], Hongmei Yu [a,*], Junbo Hou [a,b], Wei Song [a,b], Zhigang Shao [a], Baolian Yi [a]

[a] *Fuel Cell system and Engineering Laboratory, Dalian Institute of Chemical Physics, Chinese Academy of Sciences, 457 Zhongshan Road, Dalian 116023, PR China*
[b] *Graduate University of Chinese Academy of Sciences, Beijing 100039, PR China*

Received 29 September 2007; received in revised form 10 November 2007; accepted 12 November 2007
Available online 21 November 2007

Abstract

The effect of water generation on the performance of proton exchange membrane fuel cell (PEMFC) was investigated by using a periodical linear sweep method. Three different kinds of *I–V* curves were obtained, which reflected different amount of water uptake in the fuel cell. The maximum water uptake that could avoid flooding in the fuel cell and the hysteresis of water diffusion were also discussed. Quantitative analysis of water uptake and water transport phenomena in this study were conducted both experimentally and theoretically. Results showed that the water uptake capacity for the fuel cell under no severe flooding was 27.837 mg cm^{-2}. The transient response of the internal resistance indicated that the high frequency resistance (HFR) lagged the current with a value of about 20 s. The effect of purging operation on the internal resistance of the fuel cell was also explored. Experimental data showed that the cell experienced a continuous 8-min purging process can maintain at a relatively steady and dry state.

Keywords: Water transport; Transient; Proton exchange membrane fuel cell (PEMFC); High frequency resistance (HFR)

1. Introduction

Proton exchange membrane fuel cell (PEMFC) is considered to be one of the most promising power supply systems for electrical vehicles due to its high power density, cleanness of production and friendly environmental adaptability. In recent years, there has been an explosive growth in the research of this field, such as the optimization of catalyst [1–5], design of operating parameters [6–9], management of water transport and heat utilization [10–21]. Water is one of the most important factors in the PEMFC operation because the performance of a PEMFC depends strongly on the water balance within the cell. As it is well known, electro-osmotic drag and back diffusion in the membrane affect the water distribution in the PEMFC competitively.

Although the water uptake and water transport characteristics in the fuel cell is important, few studies in this field have been reported. The reasons are as follows: firstly, some parameters can hardly be obtained precisely by experiment, such as the electro-osmotic drag coefficient and the water amount due to back diffusion; secondly, there are also some design difficulties. For example, microprobes should be put into the different part of the fuel cell in order to measure the water distribution in the whole cell, but this method might destruct the original sealed structure and lead to the leaking issues. Karan et al. [11] investigated the overall water transport characteristics experimentally by collecting the outlet water at both the anode side and cathode side. They also discussed the effect of micro porous layer (MPL) on the net water transport by comparing the net water drag coefficient between the PEMFCs with and without a MPL. Results showed little difference in the net drag coefficient of the cells with a MPL between that of the cells without a MPL due to inherent variability in performance of fuel cell (FC) builds and measurement errors.

In recent years, visualization experiments were reported in which the "transparent" flow fields were used to show the liquid water formation at the gas diffusion layer (GDL) and water droplet growth in the gas channel. Yang et al. [16] and Ge et al.

* Corresponding author. Tel.: +86 411 84379051; fax: +86 411 84379185.
E-mail address: hmyu@dicp.ac.cn (H. Yu).

0378-7753/$ – see front matter © 2007 Elsevier B.V. All rights reserved.
doi:10.1016/j.jpowsour.2007.11.034

[17] showed the droplet formation and water transport at the cathode side and the anode side respectively. According to their results, as for the cathode side, liquid water was prone to emerge at the GDL and can grow to a size comparable to the channel dimension, but for the anode side, no water droplet can be observed at the anode gas diffusion layer but in the gas channel. Besides the visualization method, some other analytical techniques were also conducted in the research of water uptake and water transport characteristics in the PEMFC, such as scanning electron microscopy [18], nuclear magnetic resonance microscopy [19], neutron imaging [20], and fluorescence microscopy [21].

Model simulations were also used to predict the water transport and distribution characteristics. Um and Wang [14] applied the unified water transport model to three-dimensional fuel cells to predict water content profiles across the ionomer membrane. They found that counter-flow design benefited the water distribution in the fuel cell under low humidity conditions. Chen et al. [15] proposed a five-layer model to investigate the steady state and transient water distribution characteristics in different part of the FC, i.e., GDL, catalyst layer (CL) and membrane. Results indicated that water profile in these layers varied with the steady state current density, membrane thickness, GDL porosity, and there was an abrupt water profile jump in the GDL and CL at both the anode side and the cathode side.

In this work, we investigated the effect of the generated water on the PEMFC performance. Water accumulated in the FC was obtained by using a periodical linear sweep method. By collecting the outlet water carried out by the outlet gases and doing the water balance analysis, we compared our experimental results with the theoretical value. The evolution of *I–V* curve during the water accumulation was also discussed by the analysis of the high frequency resistance (HFR) of the fuel cell.

2. Experimental

2.1. Fuel cell setup

A commercial catalyst coated membrane Umicore® (pMembrain™ H300) was sandwiched by polytetrafluoroethylene (PTFE) -proofed GDL (Toray TGP-H-060) and hot-pressed to form a membrane-electrode-assembly (MEA). The parallel flow field was machined on the graphite bipolar plate, and the assembly was then tightened using polycarbonate endplates, bolts and nuts. The effective area of the fuel cell is only 1 cm^2.

The fuel cell was connected to a fully computer-controlled home-made test station. The cell was preconditioned by operating with fully humidified hydrogen and oxygen at 60 °C and ambient pressure for 8 h. KFM2030 (Kikusui, Japan) was used as the electric load and impedance meter in the testing process.

2.2. Experimental procedure and measurements

After precondition of the FC, in order to diminish the influence of the residual water in the fuel cell, the cell was then purged by dry hydrogen and oxygen respectively until the HFR of the FC reached a relatively steady value, in which state it was considered there was only the structural water [13] exist in the membrane. During this process, the anode and the cathode side were first purged with unhumidified H_2 and O_2 (relative humidity for H_2 and O_2 are 45%), respectively at a flow rate of 100/100 ml min^{-1} for 5 min, and then a small flow rate of 10/10 ml min^{-1} for 3 min. The HFR of the cell was recorded during this purge operation. The cell was kept at 55 °C during the whole purging process and the succeeding sweeping process.

For the ramp sweeping process, counter-flow design and unhumidified H_2 and O_2 were used. The relative humidity is 45% for both the H_2 and O_2. Water generation and accumulation in the cell was obtained by means of the rapid linear *I–V* sweep method as described by Yu and Ziegler [22]. The flow rates for both H_2 and O_2 are 10 ml min^{-1}. *I–V* sweep settings for the testing process were 0A-1A-0A, 0A-1.2A-0A, 0A-1.4A-0A, sweep rate is kept at 25 mA s^{-1}. HFR measurements were carried out at 10 kHz during all the experiments.

In order to collect the outlet water at the anode side and the cathode side, the outlets of the respective gases were connected to tubes filled with silica gel. Gravimetric analysis and water balance calculations were conducted after the sweeping cycles.

3. Results and discussion

3.1. Purging process

Gas purging operation of PEMFC has been investigated by many groups considering different pivots [23–25]. In this work, unhumidified H_2 and O_2 were used to purge the cell as dry as possible in order to remove the residual water in the PEMFC, i.e. liquid water in the gas channel, GDL and CL at both the anode and cathode side was purged, and only the structural water in the membrane and CL was regarded to exist.

Fig. 1a and b show the variation of HFR during the continuous 8-min purging process. Fig. 1a indicates the first 5-min 100/100 ml min^{-1} duration. Because the effective area of the cell is only 1 cm^2, 100/100 ml min^{-1} is relatively a high stoichiometry for this small MEA. At this flow rate, most of the residual water in the fuel cell can be purged. Two "steps" are obtained in this purging process. This phenomenon can be ascribed to different water transport characteristics in different parts of the fuel cell. As the saturation level decreases, the internal resistance increases gradually until most of the water in the catalyst layer was removed. Consequently, the first "step" refers to the water removing process in the CL, since the HFR change reflects the saturation of the Nafion® only, the first "step" does not reveal the water removal in the flow-filed and gas diffusion layer. The second "step" indicates the water removing process in the membrane. After the majority of the water in the membrane is purged, the internal resistance of fuel cell maintains at a relatively stable value. In this state, a high HFR of 1.1 Ω cm^2 is reached which reveals the dehydration of the MEA reaches a peak, and only the structural water which cannot be removed by the purging process is left in the cell. Fig. 1b shows the succeeding 3-min 10/10 ml min^{-1} purging process. The HFR decreases quickly to a relatively steady state of 435 mΩ cm^2 after about 100 s. In the presence of gas flows, although most of the liquid water

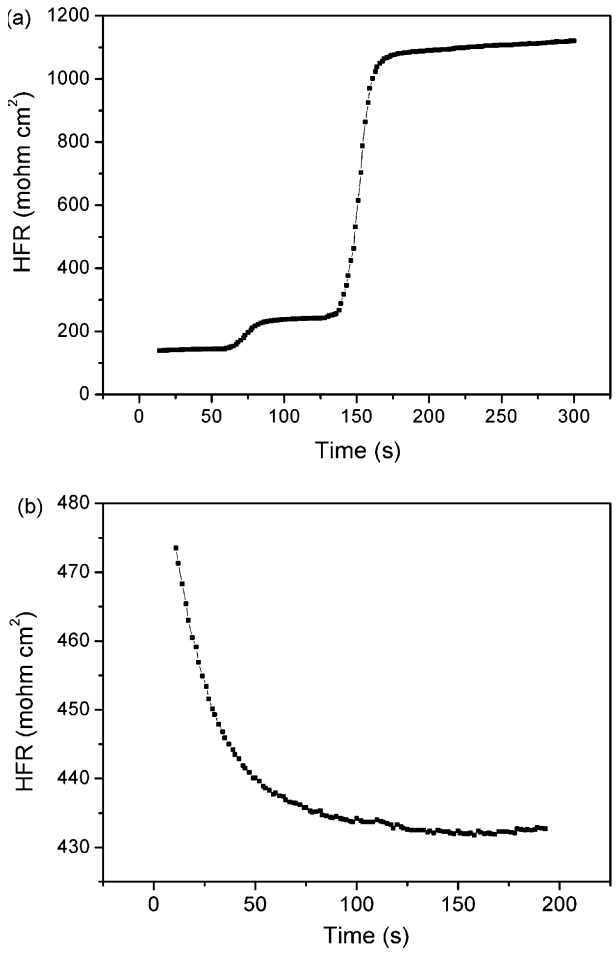

Fig. 1. Variation of the internal resistance of the fuel cell during the purging process: (a) first 5-min. 100/100 ml min^{-1} and (b) latter 3-min 10/10 ml min^{-1}.

is purged out from the MEA, the water concentration gradient does exist due to the diffusion resistance caused by the flows (i.e., a lower concentration in the CL/membrane interface and a higher water concentration in the membrane). The higher the flow rates, the bigger the concentration gradients. As the gas flows switch from 100/100 to 10/10 ml min^{-1}, the concentration gradient decreases and thus lead to a more uniform water distribution and the decrease of the HFR. As it is well known, the water content (λ) in the membrane depends strongly on the water uptake level [13,19,23,26,27], and for the well-hydrated membrane which was humidified with water vapor, λ was reported to vary from 12 to 16.8 [19,26,27]. Here, in this work, we take the water content (λ) in the membrane and CL as 14 before the purging process [27] and as 6 after the purging operation [26] by considering the membrane thickness and the water uptake capacity loss during the MEA fabrication. Noted that the flow rate of 10/10 ml min^{-1} is the same as we use in the following *I–V* sweeping process, the state after the 8-min purge is regarded as the basic state of the following sweeping tests.

3.2. Water generation in the fuel cell

After the cell is purged and reached the basic state, the *I–V* sweeping tests are conducted to investigate the water uptake capacity of the fuel cell. In this part, we will discuss the experimental phenomena only, and the quantitative analysis will be discussed in the next part. Figs. 2–7 show the evolution of *I–V* characteristics and HFR as the water accumulating in the fuel cell gradually. In Figs. 2–7, (a) indicates the *I–V* performance and (b) represents the variation of the HFR during this sweep cycle. Mainly three different kinds of *I–V* curves are observed during our cycles. Fig. 2 is the first cycle of the sweep in which the cell is just purged to the basic state. We can see that the backward *I–V* curve stands obviously above the forward one in Fig. 2a, and we label this "uptake". It indicates the hydration level of the MEA is improved greatly by the generated water in this cycle, Fig. 2b displays that the internal resistance decreases to a relatively low value which is comparable to the value that is fully hydrated in our latter cycles. It implies that water generated in the CL/membrane interface in the first cycle rehydrates the membrane to a relatively saturated level. Figs. 3 and 4 also belong to this "uptake" type, but we can see that the backward curves stay much more closer to the forward ones than the one in Fig. 2a, and so does the internal resistance of the fuel cell. This indicates the hydration level of the MEA reaches to a relatively high status but the MEA is still not fully saturated, because the

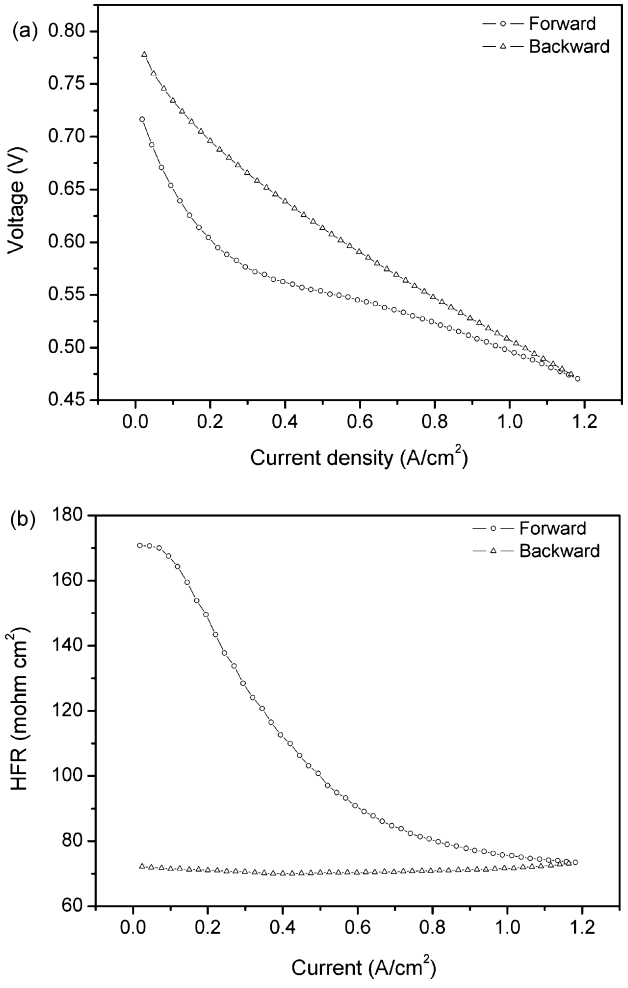

Fig. 2. The variation of (a) *I–V* performance and (b) internal resistance during the first sweeping cycle.

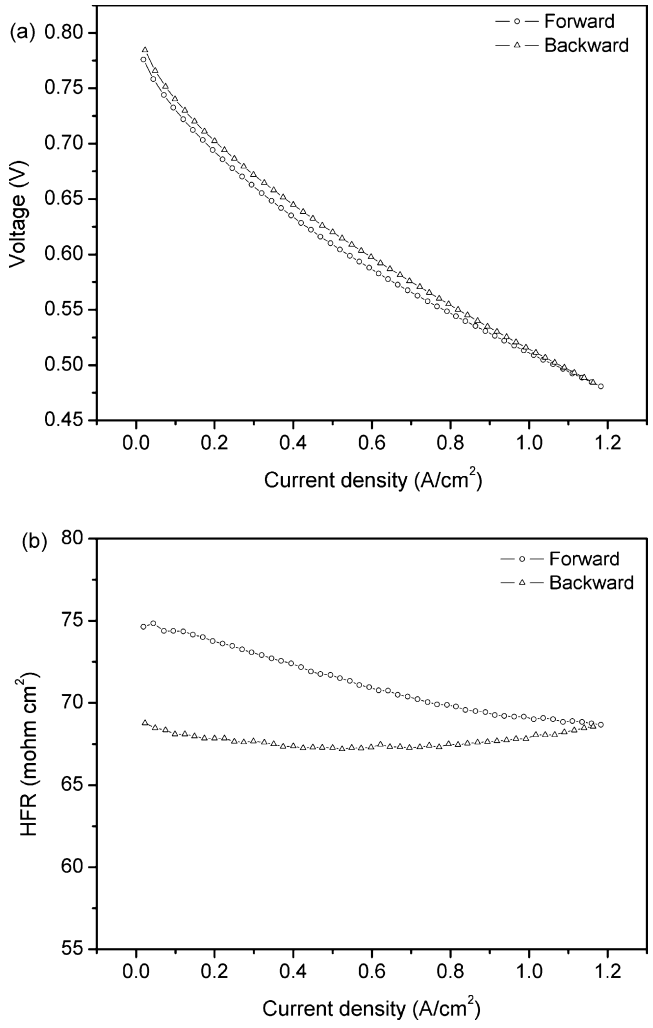

Fig. 3. The variation of (a) *I–V* performance and (b) internal resistance during the second sweeping cycle.

I–V performance of the backward sweeping process is improved as more water is accumulated in the fuel cell.

Figs. 5 and 6 reveal another kind of *I–V* curve, in which the backward sweep intersects the forward one in the medium current density in which resulting a "∞"-like curve and we label this a "threshold". In this type, the backward sweep curve stands beneath the forward one in the high current density region (above 1 A cm^{-2}) and surpass it in the low current density region (less than 0.6 A cm^{-2}). The internal resistance of the FC changes a little in Figs. 5b and 6b during these two sweeping cycles (almost remains at an average value of 65 mΩ cm^2). The small increase of the HFR during the forward sweep indicates the stronger electro-osmotic drag effect of larger current densities dehydrates the membrane of the anode side. It indicates the rehydration level of the MEA is prone to reach the fully saturated state. As it is known, more water generates in higher current density zone than the lower zone, and it will take a few seconds for water to diffuse from CL/membrane interface to other parts in the MEA. As a result, partially flooding in the high current density region with a fully saturated MEA is ineluctable when water is just generated and does not have enough time to distribute homogeneously. As less water generates during the backward sweep cycle and the distribution of generated water becomes homogeneous in each part of the cell, the backward *I–V* performance surpasses the forward one again in the lower current density zone. By comparing Figs. 5a and 6a, we can see the flooding zone becomes much larger in Fig. 6a, which means the water accumulated in the cell nearly reaches its maximum capacity.

Fig. 7 shows the third kind of *I–V* curve during the sweeping cycles. An obviously flooding phenomenon is observed in the backward sweeping process of Fig. 7a, and this is consistent with our above-mentioned analysis. Water accumulated in the fuel cell has reached its limited capacity, which means MEA cannot take anymore water generated in the sixth cycle, and thus the excessive amount of water in the GDL surface and the flow field blocks the gas transport channel to the CL interface and leads to a severe flooding phenomenon.

The three different kinds of *I–V* curves reflect the water uptake level of the MEA and gas transport characteristics in the fuel cell, but not all of these three curves would appear at any operating conditions. Fig. 8 shows the effect of flow rates on the water removability in the FC. Three different flow rates are applied during the sweeping tests, and for each flow rate we conducted five 0A-1A-0A cycles. Only the fifth cycle is shown for clarity

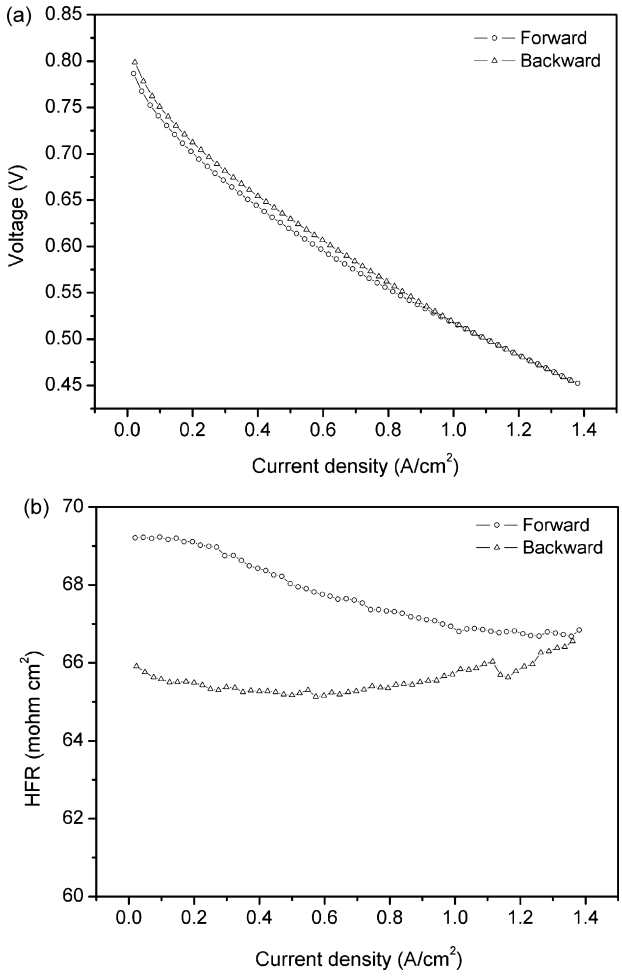

Fig. 4. The variation of (a) *I–V* performance and (b) internal resistance during the third sweeping cycle.

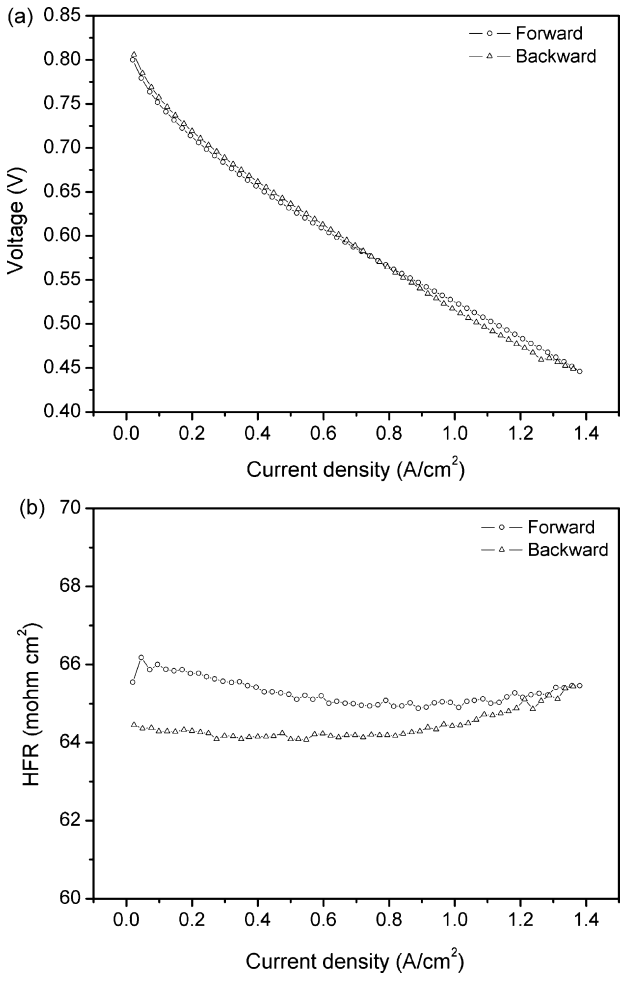

Fig. 5. The variation of (a) *I–V* performance and (b) internal resistance during the fourth sweeping cycle.

and Fig. 8 (a), (b), and (c) represents the *I–V* performance under the flow rate of 10/10, 15/15, and 20/20 ml min^{-1}, respectively. As it can be seen, a relatively dry state "uptake" type is observed except in Fig. 8a, it indicates that water accumulation in the FC is very difficult to accomplish under the flow rate of 15/15 and 20/20 ml min^{-1}. At these conditions, most of the generated water is carried out by the outlet gases. Fig. 8a shows the "threshold" type and it attributes to the accumulated water in the GDL and flow field blocks the gas transportation and results in the local flooding, which means water can accumulate in the FC during the sweeping cycles under the flow rate of 10/10 ml min^{-1}. It also indicates the "threshold" would only be obtained in the condition that the generated water can accumulate in the FC and the accumulated water can hydrate the MEA to a well-saturated state.

3.3. Water uptake capacity of the fuel cell

To understand the effect of water uptake on the *I–V* performance of the fuel cell, it is instructive to quantify the water in the fuel cell during the sweeping process. Mainly, there are three individual terms in the water balance analysis, (i) water brought in by the inlet gases $m_{H_2O,in}$; (ii) water generated during the sweeping cycles $m_{H_2O,gen}$; (iii) water carried out by the outlet gases $m_{H_2O,out}$. (i) and (iii) include both the anode and the cathode side. For term (i), the inlet H_2 and O_2 are both unhumidified gases with no liquid phase, so we can quantify $m_{H_2O,in}$ by measuring the relative humidity (RH) of the inlet gases (see Eqs. (1) and (2)). $m_{H_2O,gen}$ can be calculated by the integration of the *I–t* curve (Eq. (3)) and $m_{H_2O,out}$ is obtained by collecting the water carried out by the outlet gases. The water balance equation is shown in Eq. (4).

$$m_{H_2O,in} = n_{H_2O,in} M_{H_2O} = \frac{PV}{RT} M_{H_2O} \quad (1)$$

$$V = \frac{P}{P_{total}} V_{total} = \frac{RH P_{sat}}{P_{total}} V_{total} \quad (2)$$

$$m_{H_2O,gen} = \frac{Q_{total}}{2F} M_{H_2O} = \frac{\int_o^t i dt}{2F} M_{H_2O} \quad (3)$$

$$m_{H_2O,cell} = m_{H_2O,in} + m_{H_2O,gen} - m_{H_2O,out} \quad (4)$$

where $m_{H_2O,in}$ is the mole quantity of water, M_{H_2O} the molecular weight of water (18 g mol^{-1}), P the partial pressure of water, V the volume of water vapor, R the gas constant (8.314 Pa m^3 mol^{-1} K^{-1}), T the temperature of inlet gases

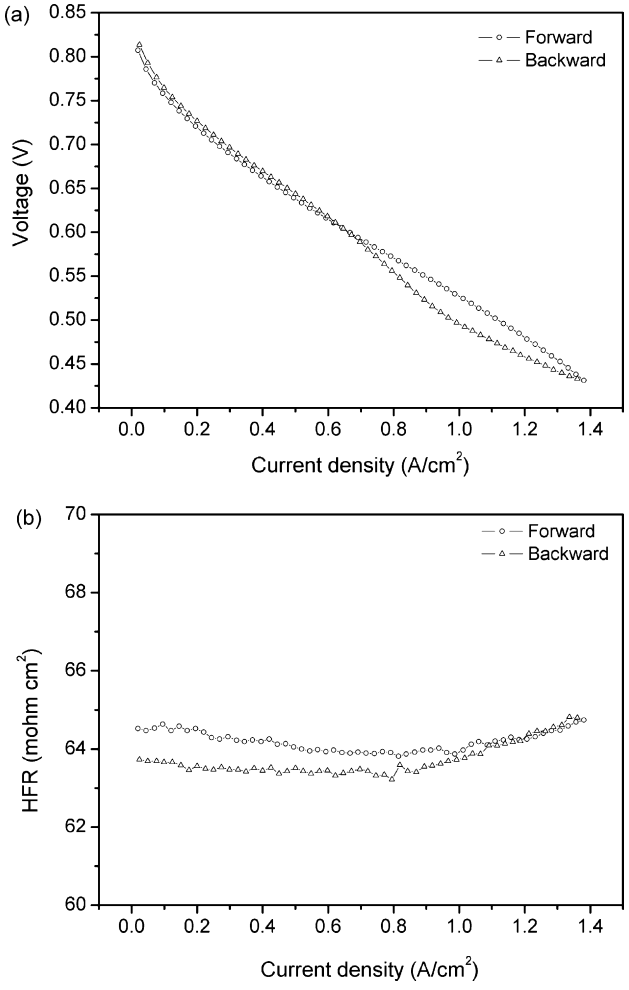

Fig. 6. The variation of (a) *I–V* performance and (b) internal resistance during the fifth sweeping cycle.

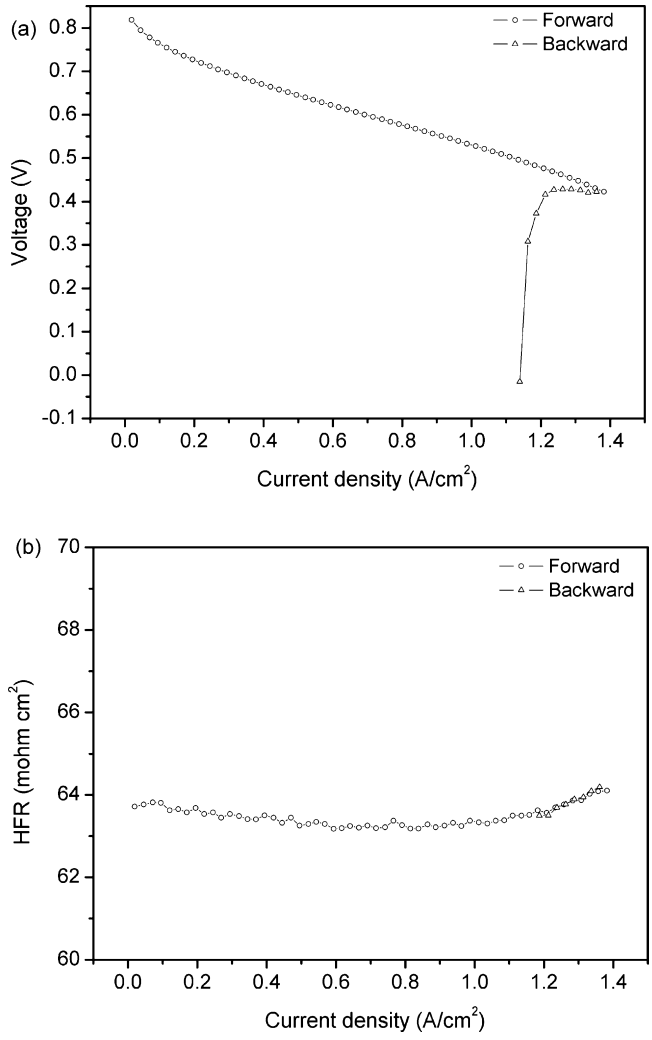

Fig. 7. The variation of (a) *I–V* performance and (b) internal resistance during the sixth sweeping cycle.

(25 °C for both sides), P_{total} the pressure of inlet gases (ambient pressure), RH the relative humidity (45% for both of the H_2 and O_2), P_{sat} the saturated vapor pressure (3167.2 Pa for 25 °C), V_{total} the total volume of the inlet gas (H_2 and O_2, respectively), Q_{total} the total charge quantity, F the Faraday constant (96485 C mol^{-1}), i the current and $m_{H_2O,cell}$ is the water uptake of the fuel cell.

For the small cell with an effective area of only 1 cm^2, we conducted five cycles in one sweeping process and did the average operation after the test in order to minimize the experimental error. Sweeping parameters are set to 0A-1A-0A with a sweeping rate of 25 mA s^{-1}. The variation of time-dependent *I–V* during the sweeping process is shown in Fig. 9. The duration of the sweeping operation is 854 s (14.23 min). The total amount of water brought in by the inlet gases calculated from Eqs. (1) and (2) is only 0.084 mg cm^{-2} in one cycle (0A-1A-0A), and the water generated in one cycle by means of integration of Fig. 9 and Eq. (3) is 7.854 mg cm^{-2}. The experimental data collected by the silica gel which represents the amount of water carried out by the outlet gases are depicted in Table 1. Both of these two processes contain five 0A-1A-0A sweeping cycles, by taking the

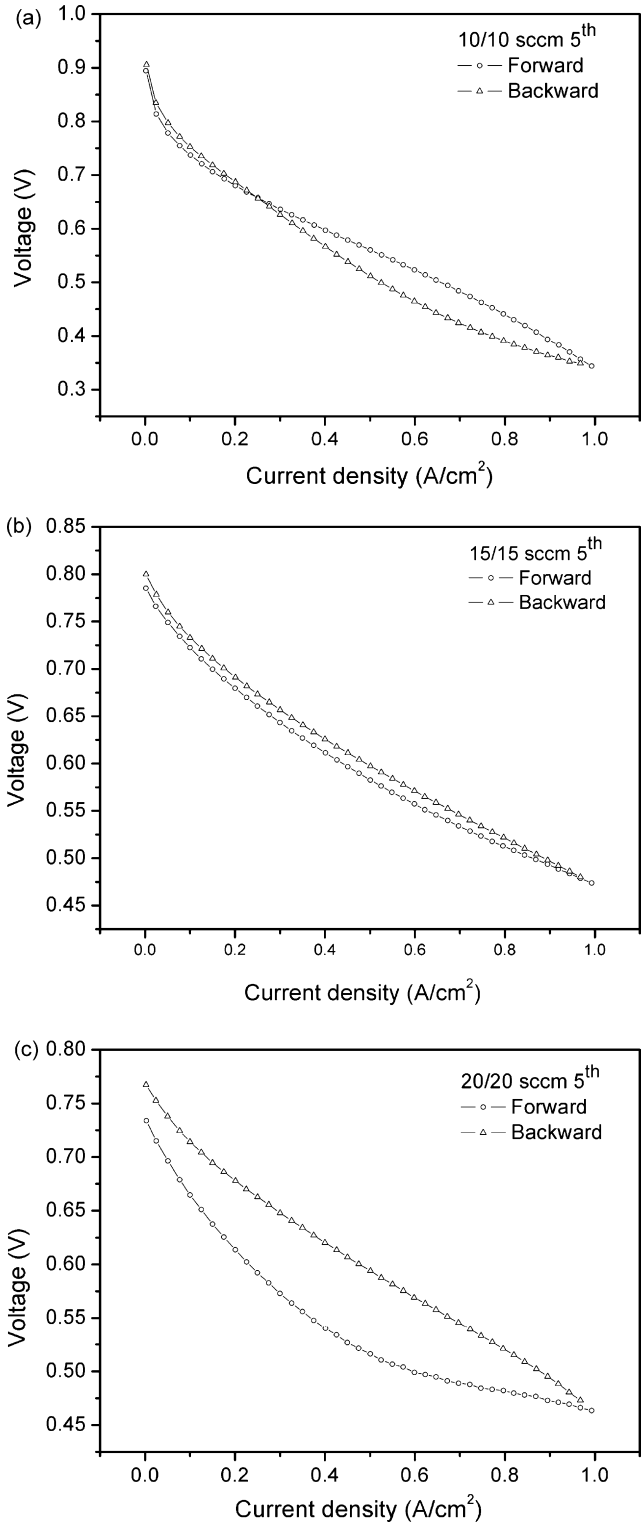

Fig. 8. Effect of flow rate on the water removability: (a) 10/10 ml min^{-1}, (b) 15/15 ml min^{-1} and (c) 20/20 ml min^{-1}.

average operation, it indicates most of the outlet water is carried out by the cathode reactant gas (H_2: 1.45 mg, O_2: 7.3 mg for one five 0A-1A-0A cycles). The total amount of water carried out in one 0A-1A-0A cycle is (1.9 +1.6) mg/2, i.e., 1.75 mg cm^{-2}, so the water uptake of the fuel cell calculated from Eq. (4) is

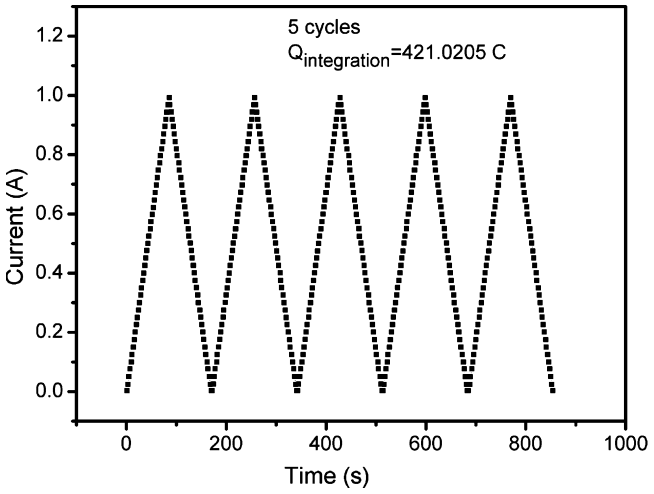

Fig. 9. Integration of the total charge quantity during the five sweeping cycles.

6.186 mg cm^{-2} for one 0A-1A-0A cycle. Considering the large flooding zone appears in the fifth cycle of our experiment, and the fuel cell is well operated in the 4–5 sweeping cycles but broken down quickly in the next sweeping procedures, it is regarded that water accumulated during the 4.5 cycles is the maximum water uptake capacity of the fuel cell, which is 27.837 mg cm^{-2}.

For further investigation on the distribution of accumulated water in each part of the MEA, the water storage capacities of the GDL, CL and membrane are estimated by the method described by Ge and Wang [23], the relating equations are depicted as follows

$$W_{\mathrm{GDL}} = \delta_{\mathrm{GDL}}\varepsilon_{\mathrm{GDL}}\eta\rho_{\mathrm{water}} \quad (5)$$

$$W_{\mathrm{cap,CL}} = \delta_{\mathrm{CL}}\varepsilon_{\mathrm{CL}}\rho_{\mathrm{water}} + \delta_{\mathrm{CL}}\varepsilon_m c_{f,\mathrm{dry}}\Delta\lambda_{\mathrm{avg,CL}}M_{\mathrm{H_2O}} \quad (6)$$

$$W_{\mathrm{cap,mem}} = \delta_{\mathrm{m}}c_{f,\mathrm{dry}}\Delta\lambda_{\mathrm{avg},m}M_{\mathrm{H_2O}} \quad (7)$$

where the symbol captions and geometrical parameters are listed in Table 2. The calculated water storage capacities of GDL, CL and membrane are 25.65, 1.31 and 0.65 mg cm^{-2}, respectively, and the total storage capacity of MEA is 27.61 mg cm^{-2}. This consists well with the experimental value of 27.837 mg cm^{-2}. What's more, in the first sweeping cycle after the purging process, we observed a quickly decrease of HFR as shown in Fig. 2b and we contributed this to the well rehydration of the membrane during the forward sweep in the first cycle. The water amount is 1.75 mg cm^{-2}/2 (0.875 mg cm^{-2}), compared with the water storage capacity of the membrane 0.65 mg cm^{-2}. It indicates that the majority of water accumulated in the first forward sweeping process is used to rehydrate the membrane, and as the sweeping cycles continue, the water generated in the cathode catalyst layer gradually distributes in the CL and GDL which results in the improvement of the *I–V* performance and decrease of the HFR until the flooding happens.

Table 1
Gravimetric analysis of collected water after five sweeping cycles

Term	Measured weight mg^{-1}	
	First	Second
Anode side	2.3	0.6
Cathode side	7.2	7.4
Total (five cycles)	9.5	8
Average (one cycle)	1.9	1.6

Table 2
Geometric parameters of the MEA

Parameter	Value
GDL thickness, δ_{GDL}	190 μm
GDL porosity, $\varepsilon_{\mathrm{GDL}}$	0.75
Volume ratio of micropores (<0.2 μm), η	0.9
Density of liquid water, ρ_{water}	1×10^3 kg m^{-3}
CL thickness, δ_{CL}	10 μm
CL porosity, $\varepsilon_{\mathrm{CL}}$	0.33
Volume fraction of ionomers in CL, ε_{m}	0.2
Fixed charge concentration in dry Nafion® ionomers, $c_{\mathrm{f,dry}}$	1.818×10^{-3} mol cm^{-3}
Difference in the average water content before and after sweeping cycles in CL, $\Delta\lambda_{\mathrm{av,CL}}$	8 (before: 6, after: 14)
Difference in the average water content before and after sweeping cycles in membrane, $\Delta\lambda_{\mathrm{av,mem}}$	8 (before: 6, after: 14)
Membrane thickness, δ_{m}	25 μm
Molecular weight of water, $M_{\mathrm{H_2O}}$	18 g mol^{-1}

3.4. Hysteresis of HFR

Fig. 10 shows the transient response of time-dependent *I–V–*HFR. The current is controlled by the electric load, and the time-acquisition limit for this system is 1 s. It depicts that the voltage changes spontaneously with the current step, but the HFR response lags the current step with a parallel value of 20 s. Here, the time hysteresis of HFR is defined as the time difference between the maximum current density and the minimum internal resistance in the same sweeping cycle. For the fixed cell fixture, the contact resistances and the bulk resistances of GDL and endplates are considered to be constant, so the periodical change of HFR during the sweeping operation is mainly caused by the variation of the membrane hydration level. The water diffusion time constant is scaled with ($\delta_{\mathrm{m}}^2/D_{\mathrm{w}}$), where δ_{m} is the membrane thickness (25 μm in this work) and D_{w} the water

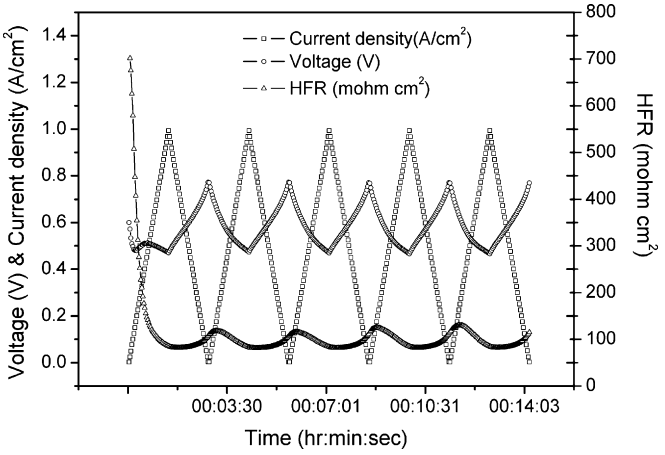

Fig. 10. Transient response of the time-dependent *I–V–*HFR.

diffusivity. D_w (for water content $\lambda > 10$) was reported [19,28–30] to vary in a range from 2.53×10^{-6} to 5.37×10^{-6} cm^2 s^{-1} considering the different membrane thickness (from Nafion® 112 to Nafion® 117). Here, we use 2×10^{-6} cm^2 s^{-1} because the membrane thickness is still less than the Nafion® 112. Thus, the diffusion time constant is about 3.1 s, which is much shorter than the experimental value of 20 s. The possible reasons are as follows: (1) the water concentration gradient is not uniform through the whole membrane surface, and the transverse equilibration of water prolongs the diffusion time; (2) the electro-osmotic effect dehydrates the membrane of anode side in the high current density zone, and thus more water will be back-diffused to the anode side. The competition between the dehydration and back diffusion takes more time to reach equilibrium. Further investigations on the time hysteresis effect is needed for the better understanding of the water transport mechanism in the MEA.

4. Conclusions

A periodical linear sweep method was used to evaluate the water uptake capacity of the proton exchange membrane (PEM) fuel cell. During the 8-min purging operation, two "steps" were observed which represent the different removability of water in CL and membrane. During the sweeping process, there were mainly three different kinds of *I–V* curves which reflect the variation of the rehydration level in the MEA. Quantitative analysis showed that the water uptake capacity of the fuel cell was about 27.837 mg cm^{-2}, and this consisted well with the theoretical value of 27.61 mg cm^{-2}. The hysteresis of HFR indicated that the water transport may be restricted by the electro-osmotic drag effect and transverse equilibration of the water content in the membrane.

Acknowledgements

This work was financially supported by the National High Technology Research and Development Program of China (863 Program, nos. 2005AA501660 and 2007AA05Z123) and National Natural Science Foundations of China (nos. 20206030 and 20636060). Kikusui Electronics Corp. is also gratefully acknowledged.

References

[1] K. Amine, M. Mizuhata, K. Oguro, et al., J. Chem. Soc. Faraday Trans. 91 (1995) 4451.
[2] E.A. Ticianelli, C.R. Derouin, S. Srinivasan, J. Electroanal. Chem. 251 (1998) 275.
[3] K. Kinoshita, J. Electrochem. Soc. 137 (1990) 845.
[4] M.-k. Min, J. Cho, et al., Electrochim. Acta 45 (2000) 4211.
[5] M.S. Wilson, S. Gottesfeld, J. Appl. Electrochem. 22 (1992) 1.
[6] S. Kim, S. Shimpalee, J.W. Van Zee, J. Power Sources 135 (2004) 110.
[7] S. Kim, S. Shimpalee, J.W. Van Zee, J. Power Sources 137 (2004) 43.
[8] Q. Yan, H. Toghiani, H. Causey, J. Power Sources 161 (2006) 492.
[9] W.H.J. Hogarth, J.B. Benziger, J. Power Sources 159 (2006) 968.
[10] A. Bazylak, D. Sinton, Z.-S. Liu, N. Djilali, J. Power Sources 163 (2007) 784.
[11] K. Karan, H. Atiyeh, A. Phoenix, et al., Electrochem. Solid State Lett. 10 (2007) B34.
[12] I. Nazarov, K. Promislow, J. Electrochem. Soc. 154 (2007) B623.
[13] H. Takata, M. Nishikawa, Y. Arimura, et al., Int. J. Hydrogen Energy 30 (2005) 1017.
[14] S. Um, C.Y. Wang, J. Power Sources 156 (2006) 211.
[15] F. Chen, M.H. Chang, C.F. Fang, J. Power Sources 164 (2007) 649.
[16] X.G. Yang, F.Y. Zhang, A.L. Lubawy, C.Y. Wang, Electrochem. Solid State Lett. 7 (2004) A408.
[17] S. Ge, C.Y. Wang, J. Electrochem. Soc. 154 (2007) B998.
[18] J. Nam, M. Kaviany, Int. J. Heat Mass Transfer 46 (2003) 4595.
[19] T.A. Zawodzinski Jr., M. Neeman, et al., J. Phys. Chem. 95 (1991) 6040.
[20] R. Satija, D. Jacobson, M. Arif, S. Werner, J. Power Sources 129 (2004) 238.
[21] S. Litster, D. Sinton, N. Djilali, J. Power Sources 154 (2006) 95.
[22] Hongmei Yu, C. Ziegler, J. Electrochem. Soc. 153 (2006) A570.
[23] S. Ge, C.Y. Wang, Electrochim. Acta 52 (2007) 4825.
[24] S.Y. Lee, E.A. Cho, J.H. Lee, et al., J. Electrochem. Soc. 154 (2007) B194.
[25] E.A. Cho, J.J. Ko, H.Y. Ha, et al., J. Electrochem. Soc. 151 (2004) A661.
[26] S. Ge, X. Li, B. Yi, et al., J. Electrochem. Soc. 152 (2005) A1149.
[27] T.A. Zawodzinski Jr., T.E. Springer, et al., J. Electrochem. Soc. 140 (1993) 1981.
[28] J.S. Pierre, J. Electrochem. Soc. 154 (2007) B88.
[29] S. Motupally, A.J. Becker, J.W. Weidnera, J. Electrochem. Soc. 147 (2000) 3171.
[30] T.E. Springer, T.A. Zawodzinski, S. Gottesfeld, J. Electrochem. Soc. 138 (1991) 2334.